European Journal of Nuclear Medicine and Molecular Imaging (2019) 46:2545–2557
https://doi.org/10.1007/s00259-019-04434-0

ORIGINAL ARTICLE

^{177}Lu-labeled low-molecular-weight agents for PSMA-targeted radiopharmaceutical therapy

Sangeeta Ray Banerjee[1,2] · Vivek Kumar[1] · Ala Lisok[1] · Jian Chen[1] · Il Minn[1] · Mary Brummet[1] · Srikanth Boinapally[1] · Michael Cole[1] · Ethel Ngen[1] · Bryan Wharram[1] · Cory Brayton[3] · Robert F. Hobbs[1] · Martin G. Pomper[1,2]

Received: 10 April 2019 / Accepted: 9 July 2019 / Published online: 10 August 2019

Abstract

Purpose To develop a prostate-specific membrane antigen (PSMA)-targeted radiotherapeutic for metastatic castration-resistant prostate cancer (mCRPC) with optimized efficacy and minimized toxicity employing the β-particle radiation of ^{177}Lu.

Methods We synthesized 14 new PSMA-targeted, ^{177}Lu-labeled radioligands (^{177}Lu-L1–^{177}Lu-L14) using different chelating agents and linkers. We evaluated them in vitro using human prostate cancer PSMA(+) PC3 PIP and PSMA(−) PC3 flu cells and in corresponding flank tumor models. Efficacy and toxicity after 8 weeks were evaluated at a single administration of 111 MBq for ^{177}Lu-L1, ^{177}Lu-L3, ^{177}Lu-L5 and ^{177}Lu-PSMA-617. Efficacy of ^{177}Lu-L1 was further investigated using different doses, and long-term toxicity was determined in healthy immunocompetent mice.

Results Radioligands were produced in high radiochemical yield and purity. Cell uptake and internalization indicated specific uptake only in PSMA(+) PC3 cells. ^{177}Lu-L1, ^{177}Lu-L3 and ^{177}Lu-L5 demonstrated comparable uptake to ^{177}Lu-PSMA-617 and ^{177}Lu-PSMA-I&T in PSMA-expressing tumors up to 72 h post-injection. ^{177}Lu-L1, ^{177}Lu-L3 and ^{177}Lu-L5 also demonstrated efficient tumor regression at 8 weeks. ^{177}Lu-L1 enabled the highest survival rate. Necropsy studies of the treated group at 8 weeks revealed subacute damage to lacrimal glands and testes. No radiation nephropathy was observed 1 year post-treatment in healthy mice receiving 111 MBq of ^{177}Lu-L1, most likely related to the fast renal clearance of this agent.

Conclusions ^{177}Lu-L1 is a viable clinical candidate for radionuclide therapy of PSMA-expressing malignancies because of its high tumor-targeting ability and low off-target radiotoxic effects.

Keywords Prostate-specific membrane antigen · β-Particle · Prostate cancer · Lutetium · Metastatic

Introduction

Prostate-specific membrane antigen (PSMA) is a type II metalloprotease and valuable clinical biomarker of prostate cancer (PC) [1, 2]. Pathology reports have revealed that over 90% of PC specimens express high levels of PSMA [3], as do most other solid malignancies [4], the latter demonstrating expression in tumor-associated neovasculature [5–7]. Lower levels are found in physiologically normal tissues such as the kidneys, salivary glands and small intestine [8]. High expression of PSMA in PC has led to its use as a target for delivering a range of diagnostic and therapeutic agents for positron emission tomography (PET), single-photon emission computed tomography (SPECT), nanoparticles and optical agents, among others [1, 9]. The PSMA-targeted, low-molecular-weight PET agents ^{68}Ga-PSMA-11 [10], ^{18}F-DCFPyL [11] and ^{18}F-PSMA-1007 [12] have revolutionized imaging-based detection of PC.

This article is part of the Topical Collection on Oncology – Genitourinary

Electronic supplementary material The online version of this article (https://doi.org/10.1007/s00259-019-04434-0) contains supplementary material, which is available to authorized users.

✉ Sangeeta Ray Banerjee
sray9@jhmi.edu

✉ Martin G. Pomper
mpomper@jhmi.edu

[1] Russell H. Morgan Department of Radiology and Radiological Science, Johns Hopkins University School of Medicine, Baltimore, MD, USA

[2] Sidney Kimmel Comprehensive Cancer Center, Johns Hopkins University School of Medicine, Baltimore, MD, USA

[3] Department of Molecular and Comparative Pathobiology, Johns Hopkins University School of Medicine, Baltimore, MD, USA

Although the recently introduced PSMA-targeted radiopharmaceuticals ^{177}Lu-PSMA-617, ^{177}Lu-PSMA-I&T [13–15] (Fig. 1a) and ^{131}I-MIP1095 [16] are promising, xerostomia remains a side effect, and long-term renal toxicity has emerged as more patients are treated more frequently and are studied over longer periods [17]. Prospective data are still lacking that address the potential issue of long-term toxicity.

We and others have investigated the pharmacokinetics of radiolabeled PSMA-targeted Lys-Glu-ureas to promote safe and effective clinical application for imaging and therapy of PC [1, 18]. So far, two general classes of high-affinity (K_i < 20 nM) agents have surfaced, which we refer to as type I and type II agents (Supplementary Figure S1). Type I agents demonstrate high PSMA-specific tumor uptake and long retention, however, with high uptake in some PSMA-expressing normal tissues including the kidney and spleen [19]. Examples include ^{99m}Tc-oxo [20], ^{64}Cu-1,4,7-triazacyclononane-1,4,7-2-triacetic acid (NOTA) [21], ^{68}Ga-PSMA-11 [22] and ^{68}Ga-/^{177}Lu-PSMA-I&T [14]. Others have recently developed several high-affinity radioligands with prolonged tumor retention using an albumin-binding 4-(*p*-iodophenyl)butyric acid motif [23–25]. That has also led to high retention in the murine renal cortex and other normal organs, indicating that such agents are type I. Type II agents display high tumor uptake and retention, and fast clearance from most normal tissues, including kidney and salivary glands, producing high tumor-to-background ratios [20, 21]. Type II agents include those developed by us [26] and PSMA-617 [13].

Here we report preclinical evaluation of a new series of theranostic ligands, ^{177}Lu-L1–^{177}Lu-L14, targeting PSMA (Fig. 1). We investigate the 4-halo-benzyl derivatives of Lys-Glu-urea because of sustained tumor uptake and high efficacy in human PC xenografts demonstrated by ^{125}I-DCIBzL (Fig. 1) [27]. Additionally, the α-particle-emitting, ^{211}At-labeled

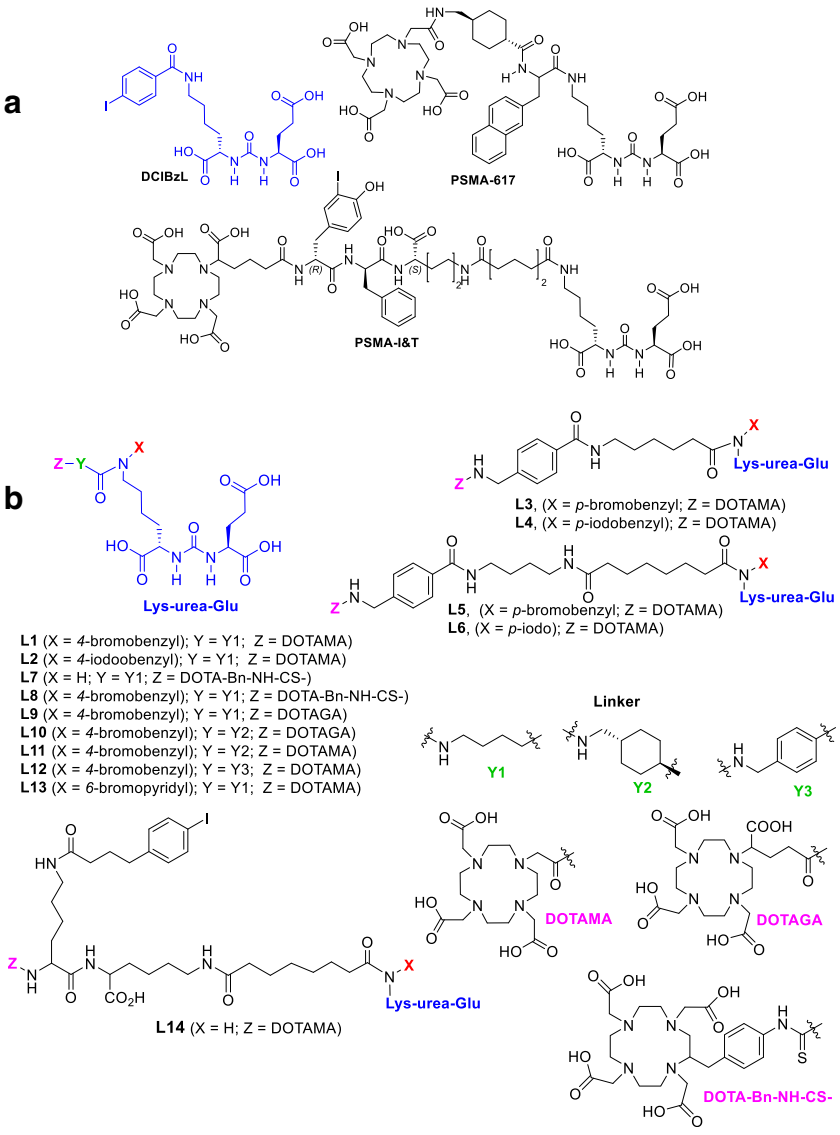

Fig. 1 **a** Chemical structures of DCIBzL, PSMA-617 and PSMA-I&T. **b** Chemical structures of the new PSMA-based compounds, L1–L14

version of DCIBzL proved effective in both flank and micrometastatic models [28]. We have synthesized 14 new ^{177}Lu-labeled radioligands and evaluated their pharmacokinetics, capacity to kill cells in vitro and tumor control in vivo. We have taken a systematic and graded approach to provide an optimized agent with reduced off-target effects for ^{177}Lu and, by extension, possibly ^{212}Pb or ^{225}Ac, each of which also utilizes a 1,4,7,10-tetraazacyclododecane-1,4,7,10-tetraacetic acid (DOTA)-based macrocyclic chelator.

Materials and methods

New compound synthesis, spectral characterization data, including a new microwave-assisted radiolabeling method, as well as cell culture and tissue biodistribution methods, are provided in the Supplementary Material. All compounds were synthesized using solution-phase chemistry based on our well-established methods [26, 29]. Ligands L1–L4, L7–L9 and L13 possess a short and flexible linker, while L10–L12 contain a rigid alicyclic or aromatic linker. In contrast, L5, L6 and L14 have a longer linker similar to our previous lead agent [26]. Binding affinities of the new ligands were determined by a competitive fluorescence-based assay reported from our laboratory [29]. All ^{177}Lu-labeled radioligands were purified by high-performance liquid chromatography (HPLC) to remove unreacted ligand from the radiolabeled material to ensure high specific radioactivity.

Cell uptake and internalization studies and clonogenic survival assay were performed as previously reported [30, 31]. Animal studies were carried out in compliance with the regulations of the Johns Hopkins Animal Care and Use Committee.

Small animal SPECT/CT imaging and histology

Single-photon emission computed tomography/computed tomography (SPECT/CT) imaging and histology were performed after administration of ^{177}Lu-L1 (37 MBq, $n = 2$–3 per time-point) via tail vein injection in PSMA(+) PC3 PIP and PSMA(−) PC3 flu flank tumor models. For SPECT/CT, we followed a previously reported method [29] with data analyzed using AMIDE software (http://amide.sourceforge.net/). Tissues were collected for histology at different time points. Hematoxylin and eosin (H&E) and immunohistochemical (IHC) staining were done as previously described by us [32]. Tumor sections were stained for γ-H2AX (phospho S139), a marker of DNA double-strand breaks, according to [33].

PSMA-targeted radionuclide therapy

Three separate in vivo treatment experiments were performed using the PSMA(+) PC3 PIP flank tumor model. Mouse body weight and tumor volume were monitored every 3 days. The formula used for calculation of tumor volume was $V = \text{width}^2 \times \text{length}/2$. Endpoint criteria as defined by the ACUC were weight loss ≥15%, tumor volume > 1800 mm^3, active ulceration of the tumor or abnormal behavior indicating pain or distress. Those definitions were also used for Kaplan–Meier analysis. For the first experiment, antitumor efficacy was evaluated for a single-dose (111 MBq) intravenous injection of ^{177}Lu-L1, ^{177}Lu-L3, ^{177}Lu-L5 ($n = 10$ mice per group), ^{177}Lu-PSMA-617 ($n = 9$) vs. saline ($n = 9$). That was a direct comparison study and employed the same batch of male NOD/SCID mice. The study was commenced 14–18 days post-inoculation of tumor cells, when tumor volumes reached ~60–85 mm^3 (Supplementary Table 21). Acute radiotoxicity of the ^{177}Lu treatment groups [(^{177}Lu-L1, ^{177}Lu-L3, ^{177}Lu-L5 and ^{177}Lu-PSMA-617 vs. saline) ($n = 3$)] after 8 weeks was evaluated at the Johns Hopkins Phenotyping Core. Mice treated with ^{177}Lu-L1 ($n = 6$) and ^{177}Lu-PSMA-617 ($n = 5$) were monitored for 190 days. The second treatment study was performed using ^{177}Lu-L1 with a variable single dose [18.5, 37 and 111 MBq vs. control ($n = 5$)] up to 80 days. A third experiment was done using single doses of ^{177}Lu-L1 of 1.9, 9.3, 18.5 MBq vs. control with saline injection ($n = 7$). Long-term radiotoxicity of ^{177}Lu-L1 (single dose, 111 MBq, $n = 3$) was assessed in immunocompetent CD-1 mice (Charles River) at 1 year after injection of the agent.

Radiation dosimetry

Murine time-integrated activity per unit of mass [TIA/g], was calculated with fits to the biodistribution data: bi-exponential for kidney and salivary glands (with physical decay constraint imposed for the salivary glands) and mono-exponential for the tumor. Conversion from TIA to absorbed dose was done using (1) a power law formula derived from a fit to spherical data generated from GEANT4 Monte Carlo for the tumor and salivary glands, and (2) the absorbed fraction from a murine kidney model, obtained by scaling the MIRD #19 kidney model [34] to murine dimensions using GEANT4 Monte Carlo for the kidneys.

Data analysis

Data are expressed as mean ± standard deviation (SD). Cell uptake and biodistribution studies were compared using the unpaired two-tailed t test. Survival analysis was performed with Kaplan–Meier curves and the log-rank test. A P value <0.05 was considered significant.

Results

Chemistry and radiochemistry

We synthesized the series of compounds for structure–activity relationships (SAR) shown in Fig. 1. All ligands bear a

bromo- or iodo-benzyl Lys-urea-Glu-targeting moiety, except for L7 and L14. The effect of chelating agent was investigated in ligands L7 and L8 by replacing DOTA-monoamide (DOTAMA), used in L1, by S-2-(4- isothiocyanatobenzyl)-DOTA (DOTA-Bn-NCS) and in L9 using DOTA-glutaric acid (DOTAGA). Ligands L10 and L11 have a rigid cyclohexyl linker, as in PSMA-617, with DOTAGA and DOTAMA chelating agents for assessing the effect of a rigid linker and choice of chelator compared to L9 and L1, respectively. Ligand L13 has a bromo-pyridyl group on the targeting urea as in our clinical PET agent, ^{18}F-DCFPyL. Ligand L14 has an albumin-binding moiety, 4-(*p*-iodophenyl)butyric acid, on our previously reported PSMA-binding targeting platform as recently studied by several research groups [23–25] to investigate the effect of 4-(*p*-iodophenyl) on biodistribution. All ligands were radiolabeled with ^{177}Lu in high radiochemical yield (> 98%) and purity (> 99%) using both conventional and microwave-assisted methods.

Affinity, cell uptake and internalization

All ligands demonstrated high binding affinity to PSMA with K_i values ranging from 0.03 to 8 nM (Table 1). The stable lutetium analog of L1 (Lu-L1) showed a threefold increase in binding affinity over L1, suggesting that all radioligands (^{177}Lu-L) of this class should also display a similar increase in binding affinity compared to the corresponding free ligand. Cell uptake and internalization data up to 24 h of incubation with ^{177}Lu-L1, ^{177}Lu-L3 and ^{177}Lu-L5 are shown in Fig. 2 and Supplementary Table 1. The total cell surface uptake and internalization of the radioligands in PSMA(+) PC3 PIP cells increased between 2 and 24 h. Both ^{177}Lu-PSMA-I&T and ^{177}Lu-PSMA-617 displayed significantly higher cell uptake within the PSMA(+) PC3 PIP cells, ~60% and ~40% of the incubated dose, respectively, compared to ^{177}Lu-L1, ^{177}Lu-L3 and ^{177}Lu-L5 initially, which showed uptake of ~30% (Fig. 2). However, the percentage of internalization for all 5 compounds was in the same range of ~18–24% at 1 h to 25–30% at 24 h of incubation. The uptake in PSMA(+) PC3 PIP cells could be blocked by treatment with an excess (~ 10 μM) of known PSMA inhibitor, ZJ43 [35], indicating binding specificity to PSMA.

Table 1 Physical properties and PSMA binding activity of the new compounds

Ligand	Molecular weight	K_i [nM]
L1	973.87	0.20–0.33 nM
L2	1020.87	0.09–34 nM
L3	1121.05	0.14–0.39 nM
L4	1168.05	0.46–0.63 nM
L5	1234.21	0.35–0.93 nM
L6	1281.21	0.29–0.81 nM
L7	970.06	NA
L8	1139.08	0.08–0.16 nM
L9	1045.94	0.02–0.05 nM
L10	1086.00	0.43–1.2 nM
L11	1013.94	NA
L12	1007.89	0.22–4.03 nM
L13	974.86	0.23–8.10 nM
L14	1390.34	0.13–2.15 nM

Cell uptake and internalization of selected radioligands from the series were assessed at 2 h post-incubation (Fig. 3a, Supplementary Table 2) and compared to ^{177}Lu-L1. DOTA-Bn-SCN-chelated ^{177}Lu-L8, with a *p*-bromo-benzyl moiety, displayed higher uptake and nearly > 1.5-fold higher internalization compared to ^{177}Lu-L7, which does not possess a *p*-bromo-benzyl group. Significantly, ^{177}Lu-L9, which is equipped with a DOTAGA chelating group, displayed higher uptake compared to ^{177}Lu-L8 and ^{177}Lu-L1. In contrast, ^{177}Lu-L10, which also employs DOTAGA, but is also modified with a rigid cyclohexyl linker, showed lower uptake and internalization compared to ^{177}Lu-L8 and ^{177}Lu-L9. Structurally unrelated radioligand ^{177}Lu-L14, with the albumin-binding 4-(*p*-iodophenyl)-butyric acid moiety, displayed highest uptake and internalization from the series at 2 h. Overall, ^{177}Lu-L8 and ^{177}Lu-L9, which differ only with respect to chelator, demonstrated significantly higher uptake in PSMA(+) PIP cells compared to ^{177}Lu-L1, while the radioligands with a rigid linker (^{177}Lu-L10, ^{177}Lu-L11 and ^{177}Lu-L12) displayed significantly lower PSMA(+) cell binding compared to similar analogs with linear linkers (e.g., ^{177}Lu-L1 and ^{177}Lu-L9).

Biodistribution

In vivo pharmacokinetics of the new compounds are presented in Figs. 2 and 3. Mouse body and tumor weights for the selected agents are provided in Supplementary Tables 3 and 4. Except for ^{177}Lu-L7, which is without the *p*-bromo-benzyl-modified Lys-Glu-urea moiety, and agents with a rigid linker (^{177}Lu-L11 and ^{177}Lu-L12), all compounds demonstrated high PSMA(+) PC3 PIP tumor uptake (>18% ID/g) at 24 h post-injection. Biodistribution of ^{177}Lu-PSMA-617, ^{177}Lu-PSMA-I&T, ^{177}Lu-L1, ^{177}Lu-L3 and ^{177}Lu-L5 are shown in Fig. 2b. At 3 h post-injection, significantly higher tumor uptake was observed for ^{177}Lu-L3 [52.6 ± 4.9% injected dose per gram (ID/g)] and ^{177}Lu-L5 (56.3 ± 18.3 %ID/g), while the tumor uptake for ^{177}Lu-L1 was comparable to ^{177}Lu-PSMA-617 and ^{177}Lu-PSMA-I&T. However, after 24 h, both ^{177}Lu-L3 and ^{177}Lu-L5 demonstrated rapid clearance from the PSMA(+) PC3 PIP tumors, ultimately providing tumor uptake comparable to ^{177}Lu-PSMA-617 and ^{177}Lu-PSMA-I&T. In contrast, ^{177}Lu-L1 displayed significantly lower tumor uptake compared to ^{177}Lu-PSMA-617 at 24 h. At 72 h post-injection, ^{177}Lu-PSMA-617 displayed higher tumor uptake compared to ^{177}Lu-PSMA-I&T, ^{177}Lu-L1 and ^{177}Lu-L3 and comparable to ^{177}Lu-L5. Uptake in the PSMA(−) PC3 flu

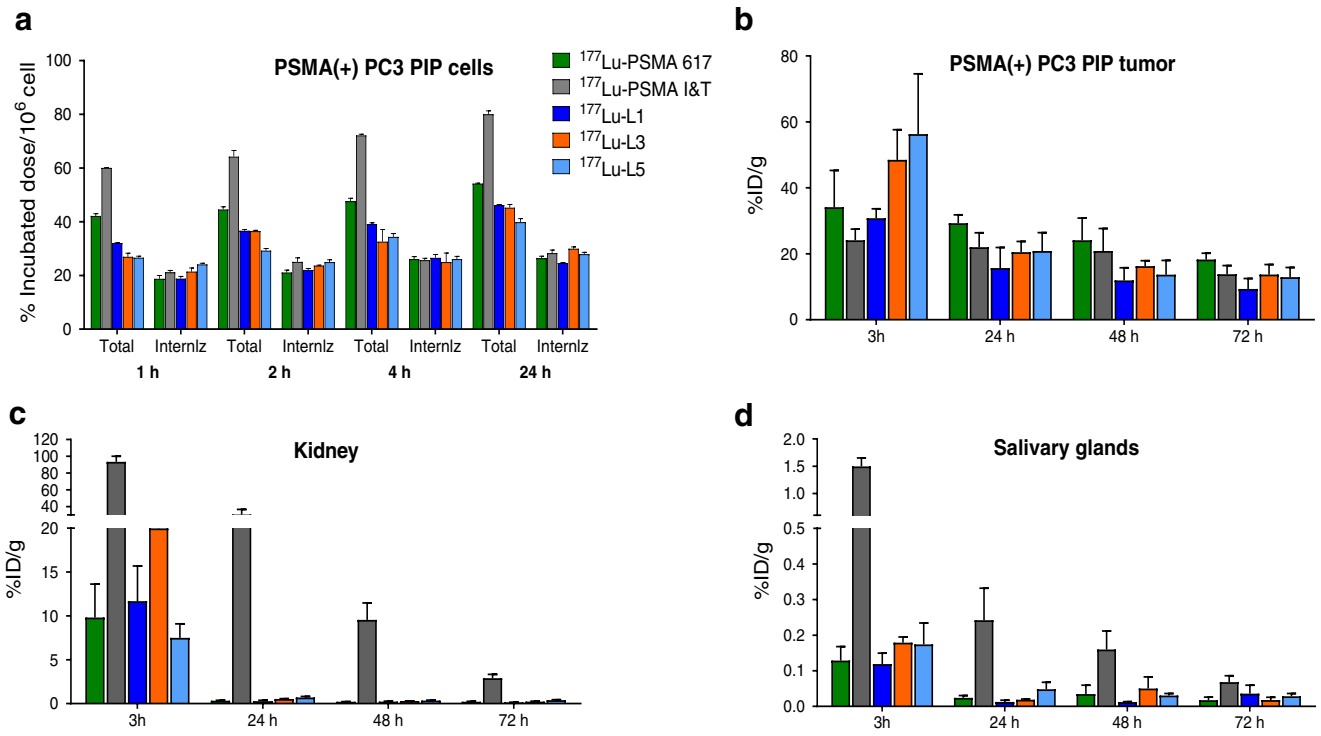

Fig. 2 **a** Cell uptake and internalization data in PSMA(+) PC3 PIP cells (percentage incubated dose per 1 million cells, mean ± SD, $n = 3$). Selected biodistribution data [PSMA(+) PC3 PIP tumor (**b**), kidney (**c**) and salivary glands (**d**)] after administration of 1.85 ± 0.37 MBq of ^{177}Lu-PSMA-617, ^{177}Lu-PSMAI&T, ^{177}Lu-L1, ^{177}Lu-L3 and ^{177}Lu-L5 (%ID/g, mean ± SD, $n = 4$ per group)

tumor was low (<0.3% ID/g) for all compounds starting at 3 h post-injection, demonstrating high specificity of the compounds tested.

Although agents tested demonstrated similar tumor uptake, they were quite different with respect to normal tissue distribution. Organs that normally express PSMA, for example, kidneys, salivary glands and spleen, showed significantly higher radiotracer uptake for ^{177}Lu-PSMA-I&T than for the other compounds. Even though ^{177}Lu-PSMA-I&T showed a certain degree of renal clearance over time, demonstrating 30.4 ± 12.5 %ID/g at 24 h, ^{177}Lu-L1, ^{177}Lu-L3, ^{177}Lu-L5 and ^{177}Lu-PSMA-617 showed an almost tenfold clearance, resulting in kidney uptake <0.5 ID/g, over the same period of time.

Selected tissue biodistribution data of ^{177}Lu-L2, the *p*-iodo-benzyl analog of ^{177}Lu-L1, and ligands without any halo-benzyl-modified urea-targeting moiety, ^{177}Lu-L7 and ^{177}Lu-L14, and *p*-bromobenzyl-modified agents, ^{177}Lu-L8, ^{177}Lu-L9 and ^{177}Lu-L10, are shown in Fig. 3b. ^{177}Lu-L2 displayed nearly similar biodistribution properties as ^{177}Lu-L1. While both ^{177}Lu-L7 and ^{177}Lu-L8 were modified with the DOTA-Bn-SCN chelating agent, tumor uptake and retention of ^{177}Lu-L8 were significantly higher at all time points compared to ^{177}Lu-L7, further emphasizing the importance of the *p*-bromobenzyl group on tumor retention. Similarly, DOTAGA-modified ^{177}Lu-L9 displayed significantly higher tumor uptake and retention compared to ^{177}Lu-L1, however, with nearly threefold higher kidney uptake at 2 h.

Biodistribution of ^{177}Lu-L14 was consistent with reported albumin-binding agents, with high and sustained tumor uptake. Although the agent initially displayed lower renal uptake compared to ^{177}Lu-PSMA-I&T, only ~ threefold clearance of activity was observed during the time course of the study, for example displaying 17.47 ± 4.18 %ID/g after 48 h, compared to a tenfold wash-out of the activity for ^{177}Lu-PSMA-I&T over that same period of time (Figs. 2 and 3). ^{177}Lu-L14 also showed the highest blood uptake from the series, 16.13 ± 2.33 %ID/g at 2 h post-injection, followed by 5.05 ± 0.05 %ID/g at 24 h and 2.48 ± 0.44 %ID/g at 48 h. Spleen salivary and lacrimal gland uptake and retention of ^{177}Lu-L14 were highest in the series.

To mitigate renal uptake, self-blocking studies were performed for ^{177}Lu-L1 and ^{177}Lu-L9. Among newly synthesized agents, those two displayed the lowest and highest kidney uptake (Fig. 3c, Supplementary Tables 19 and 20) at 2 h post-injection, respectively. Different self-blocking doses were co-administrated with radioligands compared to the control with no blocking dose. Of note, both radioligands displayed a greater than sixfold decrease in kidney uptake using ~ 0.5 nmol of blocker. Owing to its low kidney uptake, ^{177}Lu-L1 maintained comparable tumor uptake compared to unblocked (34.7 ± 8.2 vs. 38.7 ± 13.5% D/g) while demonstrating significant blockade in kidney uptake (34.74 ± 17.37 vs. 4.76 ± 1.35% D/g). ^{177}Lu-L9 also displayed significant blocking within the PSMA-expressing lacrimal and salivary glands.

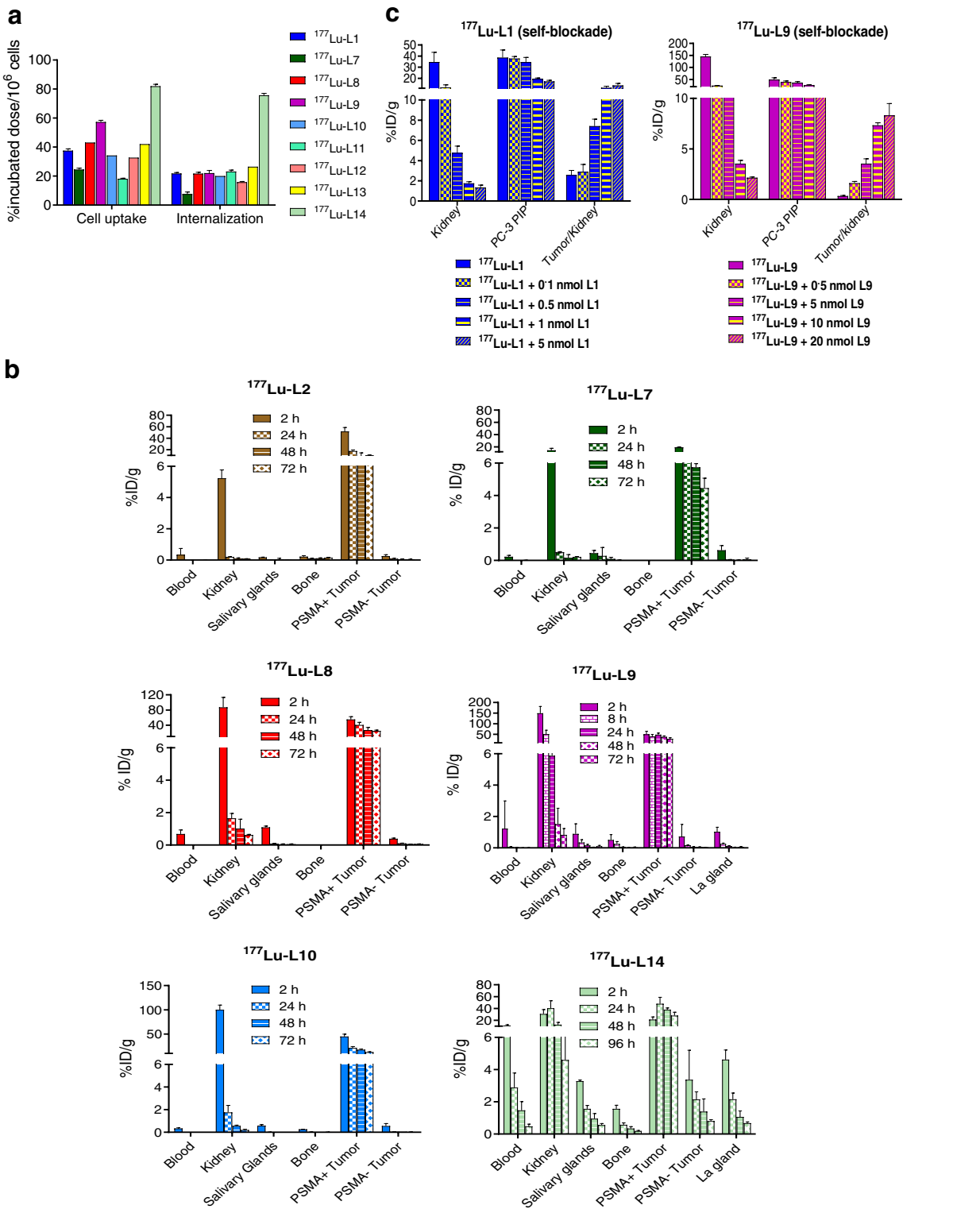

Fig. 3 **a** Cell uptake and internalization data of the selected radioligands in PSMA(+) PC3 PIP cells compared to ^{177}Lu-L1 (percentage incubated dose per 1 million cells, mean ± SD, $n = 3$). **b** Biodistribution data of ^{177}Lu-L2, ^{177}Lu-L7, ^{177}Lu-L8, ^{177}Lu-L9, ^{177}Lu-L10 and ^{177}Lu-14. **c** Self-blocking study performed of ^{177}Lu-L1 and ^{177}Lu-L9 using variables doses of the respective ligands. (%ID/g, mean ± SD, $n = 4$ per group)

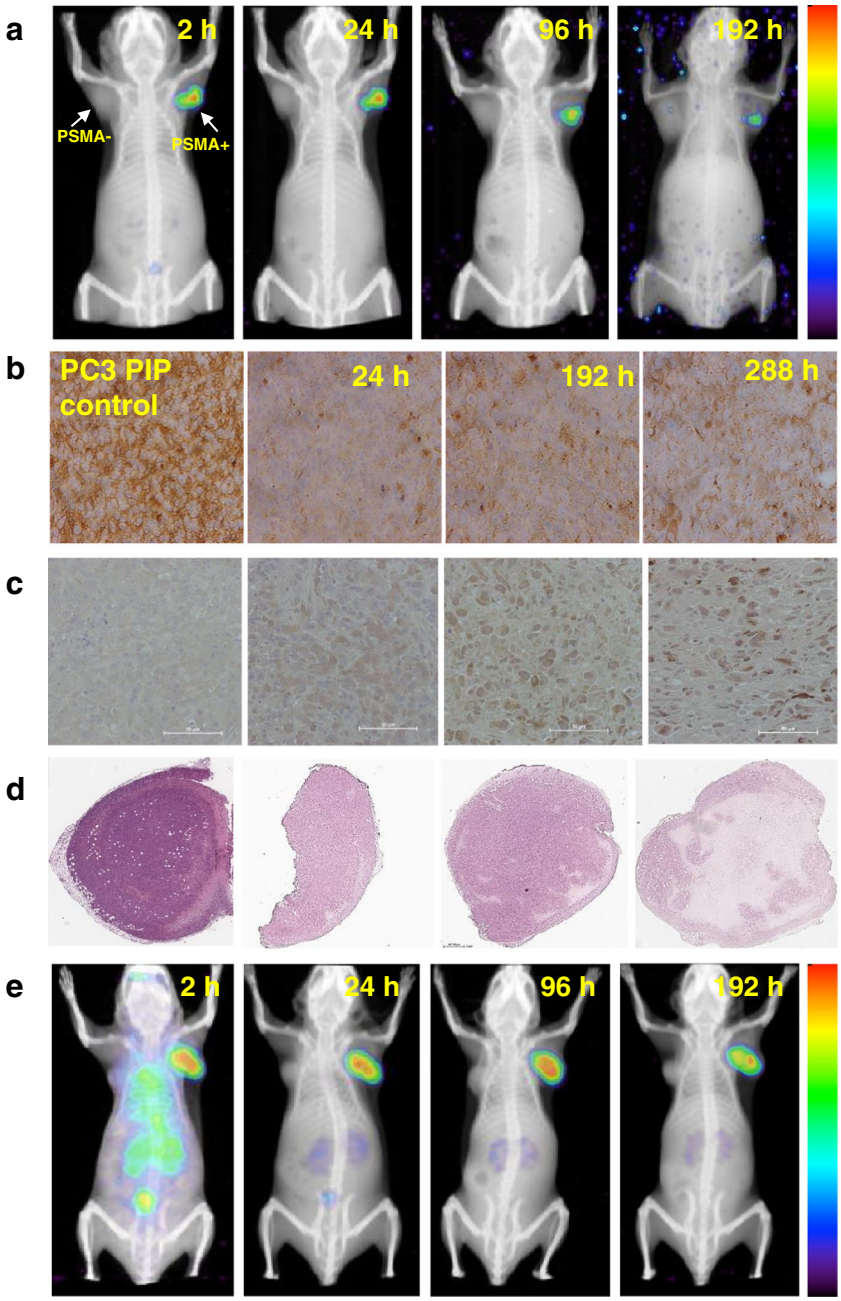

Fig. 4 **a** and **e** SPECT/CT imaging ^{177}Lu-L1 and ^{177}Lu-L14 (37 MBq) in PSMA(+) PC3 PIP and PSMA(−) PC3 flu tumor bearing mouse during 2–192 h ($n = 2$). **b** Representative IHC staining of PSMA expression. **c** γ-H2A.X staining to demonstrate DNA damage (scale bar: 50 μm, 20X). **d** H&E staining of whole tumor issue sections within the PSMA(+) PC3 PIP tumor for untreated control and after administration of ^{177}Lu-L1 24 h, 7 and 12 d (left to right) (scale bar:660μm, 2X)

Tumor imaging by in vivo SPECT/CT and ex vivo histology

SPECT/CT imaging of ^{177}Lu-L1 and ^{177}Lu-L14 (Fig. 4a and e) was also performed to check in vivo pharmacokinetics panoramically. As anticipated from the biodistribution data, SPECT/CT images during 2–192 h after administration of ^{177}Lu-L1 confirmed high uptake in the PSMA(+) PC3 PIP tumors (right) but not in the PSMA(−) PC3 flu tumors (left). Also, consistent with the biodistribution data, the ligand displayed very low uptake in kidneys and all normal tissues, including after 2 h post-administration. We also established the status of PSMA expression within the PSMA(+) PC3 PIP tumors during the imaging experiments by IHC and tumor morphology by H&E staining. We detected a decrease in PSMA expression in the PSMA(+) PC3 PIP tumors at all time points after administration of ^{177}Lu-L1 (37 MBq) compared to tumor harvested from control animals that did not receive radioactivity (Fig. 4b). This was attributed to the loss of PSMA-expressing tumor cells following effective therapy. However, there was an apparent rebound in PSMA expression over time. That rebound could represent PSMA that was internal and not available for IHC staining (or radiotherapy) at the earlier time points. Additionally, significant DNA damage

was visualized by γ-H2A.X staining at 7 d compared to 24 h and in the non-treated control. Whole-tumor H&E staining at 7 d and specifically at 12 d presented extensive necrosis within the treated tumors (Fig. 4d), indicating significant cell kill using 37 MBq of ^{177}Lu-L1. A theranostic SPECT/CT imaging study was also performed for ^{177}Lu-L8 using 111 MBq from 24 to 192 h post-treatment (Supplementary Figure 2), although pharmacokinetics were inferior to ^{177}Lu-L1.

Radionuclide therapy

The colony-forming ability of PSMA(+) PC3 PIP cells after incubation with ^{177}Lu-L1, ^{177}Lu-L3, ^{177}Lu-PSMA-617 and ^{177}Lu-PSMA-I&T is shown in Fig. 5a. Significant loss of colony formation was observed only after 48 h of incubation for all compounds. The D_0 (37% survival) of ^{177}Lu-PSMA-617, ^{177}Lu-L1 and ^{177}Lu-L3 were in the same range (24–32 kBq/mL), whereas that for ^{177}Lu-PSMA-I&T was much lower (~ 9.5 kBq/mL), as anticipated from the cell uptake data. PSMA(−) PC3 flu cells did not display any cell kill effect under similar experimental conditions for any radioligand.

To evaluate in vivo efficacy, initially, a pilot study was conducted using PSMA(+) PC3 PIP tumors with a single intravenous dose of the vehicle (control) or 111 MBq of ^{177}Lu-PSMA-617, ^{177}Lu-L1, ^{177}Lu-L3 or ^{177}Lu-L5 (Supplementary Table 21 and Fig. 5b). Kaplan–Meier survival plots, individual tumor volume and body weight measurements for each animal are shown in Supplementary Figures 3–8. The tumor volume of mice in the control group reached > 5 times the initial volume within 14 days. All treated groups showed significant tumor regression up to 8 weeks post-treatment. The survival among treatment groups was statistically significant by the log-rank test compared to the untreated group ($P < 0.0001$ for ^{177}Lu-PSMA-617 and ^{177}Lu-L1, $P < 0.001$ for ^{177}Lu-L5, and $P < 0.01$ for ^{177}Lu-L3). As shown in Supplementary Table 21, only one mouse from the group treated with ^{177}Lu-L5 or ^{177}Lu-PSMA-617 reached a relative tumor volume > 4 times the initial volume, and two mice from the group treated with ^{177}Lu-L3 progressed to that degree. The cause of death of the other mice treated with the agents in Supplementary Table 21 was due to a sudden decrease in body weight, and was not directly related to tumor growth. While treatment monitoring was terminated for ^{177}Lu-L3 and ^{177}Lu-L5 at 8 weeks, treatment was continued for ^{177}Lu-L1 and ^{177}Lu-PSMA-617 until the predefined end-point was reached. Figure 5c displays the survival data of ^{177}Lu-L1 and ^{177}Lu-PSMA-617. Median survival for ^{177}Lu-PSMA-617 was 130 days, whereas for ^{177}Lu-L1, survival was still > 60% of animals at 190 days after administration.

Toxicity was assessed initially at 8 weeks post-treatment through complete blood analysis and necropsy. Selected toxicity data are shown in Fig. 5d and Supplementary Tables S22–S24. All animals that underwent radiotherapy had normal creatinine (0.3–0.4 mg/dL) and blood urea nitrogen levels. All three mice receiving ^{177}Lu-PSMA-617 had significantly lower platelets than those in the other treatment groups. One of those mice also had the greatest tumor burden, and the highest neutrophil count of the mice tested, including possible lung metastases (<1 mm) (Supplementary Figure 13).

Anatomic pathology identified significant changes in lacrimal grands (Fig. 5e) and testes (Fig. 5f) in all treated groups. Lacrimal glands (extraorbital and infraorbital) in all treatment groups had marked degenerative, inflammatory and fibrotic changes. Salivary glands were generally spared, but mice receiving ^{177}Lu-PSMA-617 had mild changes in parotid glands. Testes of one mouse receiving ^{177}Lu-L5 and all three mice receiving ^{177}Lu-PSMA-617 had the most severe degenerative changes and loss of seminiferous epithelium. Changes in kidneys were minimal in all treated groups. One mouse receiving ^{177}Lu-L5 had thymic lymphoma, which is an expected cause of death in naïve NOD/SCID mice [36], and may be accelerated by irradiation and certain carcinogens. Possible mild changes in ameloblasts and odontoblasts were identified in limited incisor sections examined for all treated mice.

Given that ^{177}Lu-L1 demonstrated a suitable treatment effect, we performed tumor growth delay studies using escalated doses from 18.5, 37 and 111 MBq ($n = 5$ per group) up to 80 days and a separate study with lower doses (1.9, 9.3, 18.5 MBq, $n = 7$) (Figures S10–S12). As shown in Fig. 6, ^{177}Lu-L1, exhibited tumor growth delay for all treated groups except for the 1.9 MBq treatment group compared to untreated. Long-term radiotoxicity was also evaluated for ^{177}Lu-L1 after administration of 111 MBq in tumor-free CD-1 mice ($n = 3$). One treated mouse had a small (<1 mm) adenoma of the lung. That is not a surprising finding in CD-1 mice in chronic studies [37]. We speculate that the cause of the death of another mouse after 11 months most likely related to similar natural death events of CD-1 mouse of this age [37]. No

Fig. 5 In vitro and in vivo therapeutic efficacy of PSMA-targeted radioligands. **a** In vitro cell kill effect of ^{177}Lu-PSMA-617, ^{177}Lu-PSMA I&T, ^{177}Lu-L1 and ^{177}Lu-L3 after 48 h incubation in PSMA(+) PC3 PIP and PSMA(−) flu cells (data mean ± SD, $n = 3$) at 37 °C. **b** Effect of ^{177}Lu-PSMA-617 ($n = 9$), ^{177}Lu-L1,^{177}Lu-L3 and ^{177}Lu-L5 ($n = 10$) on the PSMA(+) PC3 PIP tumor growth (data mean ± SD) after administration of 111 MBq via tail-vein injection. **c** Kaplan–Meier plot of survival for the group treated with ^{177}Lu-PSMA-617 ($n = 9$) and ^{177}Lu-L1 ($n = 10$), censored event (dot), three mice were removed from each group at 8 weeks for evaluating acute toxicity. **d** Hemoglobin and blood counts (white blood cells, neutrophil and platelets) level after 8-week. Data are mean ± SD ($n = 3$). **e** and **f** Acute toxicity evaluation by H&E staining of lacrimal glands and testes. Extraorbital lacrimal glands control untreated (left); ^{177}Lu-PSMA-617(middle and right), adjacent parotid gland (arrowhead) is spared (middle); higher magnification, showing acinar loss, with chronic and active inflammation (right). Testis control untreated, active spermatogenesis, near the rete testis 2 tubules (arrowhead) contain only Sertoli cells (left), ^{177}Lu-PSMA-617 (right). Diffuse and near complete loss of seminiferous epithelium, with prominent interstitial cells

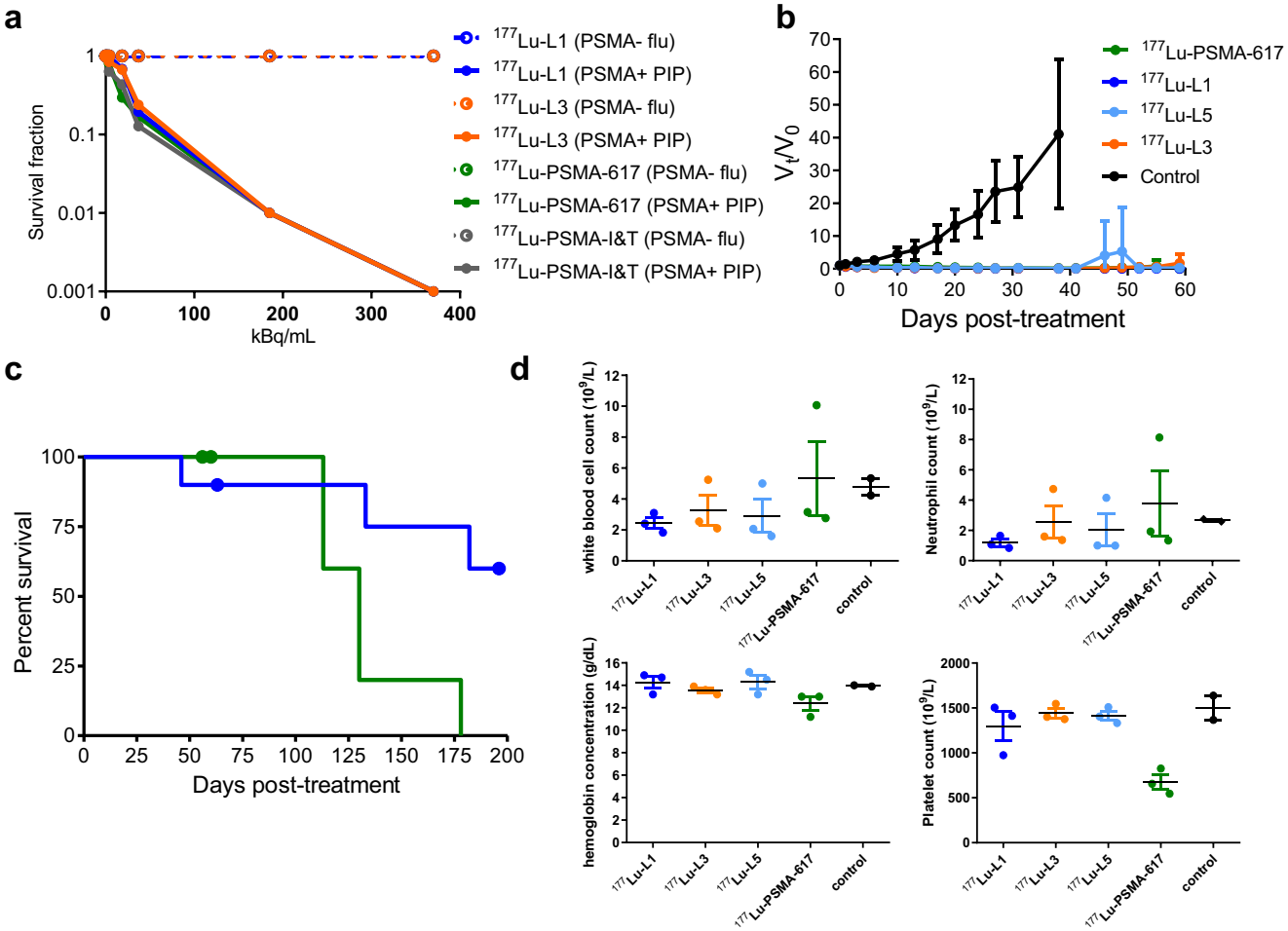
a
Survival fraction
kBq/mL
177Lu-L1 (PSMA- flu)
177Lu-L1 (PSMA+ PIP)
177Lu-L3 (PSMA- flu)
177Lu-L3 (PSMA+ PIP)
177Lu-PSMA-617 (PSMA- flu)
177Lu-PSMA-617 (PSMA+ PIP)
177Lu-PSMA-I&T (PSMA- flu)
177Lu-PSMA-I&T (PSMA+ PIP)
b
Vt/V0
Days post-treatment
177Lu-PSMA-617
177Lu-L1
177Lu-L5
177Lu-L3
Control
c
Percent survival
Days post-treatment
d
white blood cell count (10^9/L)
Neutrophil count (10^9/L)
hemoglobin concentration (g/dL)
Platelet count (10^9/L)
177Lu-L1
177Lu-L3
177Lu-L5
177Lu-PSMA-617
control

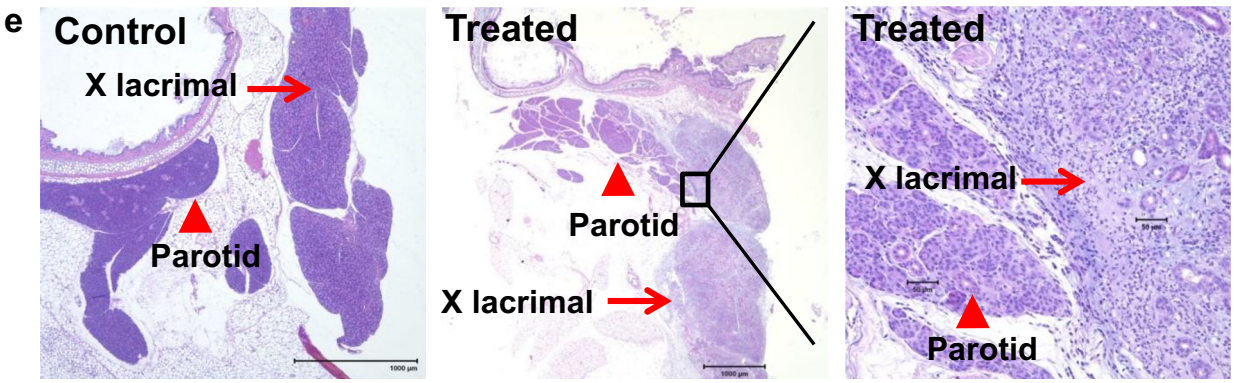
e
Control
X lacrimal
Parotid
Treated
Parotid
X lacrimal
Treated
X lacrimal
Parotid

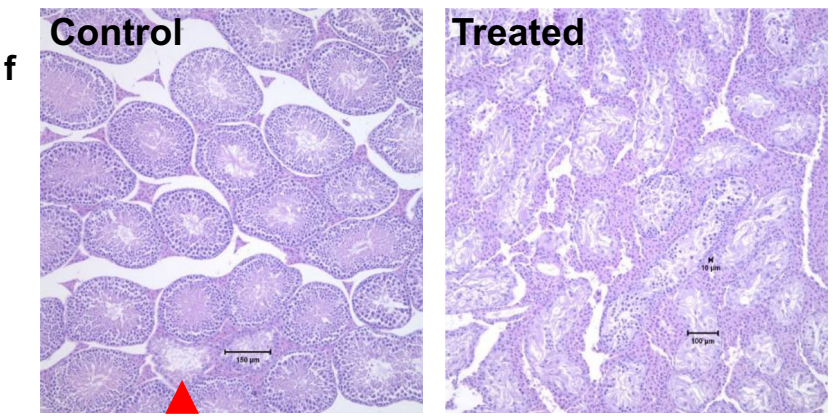
f
Control
Treated

measurable toxicity was found for the treated mice compared to controls in the kidneys with acceptable blood urea nitrogen, albumin, creatinine and total protein level [38]. In contrast to 8 weeks post-treatment, changes in lacrimal glands and testes were minimal after 1 year. Changes in adrenal glands, kidneys, urinary bladder and liver were mild, but may exceed expected age-related changes and warrant further assessment (Supplementary Figure 15 and Tables 25–26).

Organ absorbed doses

Figure 6c provides selected mouse organ absorbed dose coefficients (mGy/MBq) for ^{177}Lu-L1, ^{177}Lu-L9 and ^{177}Lu-L14. For all radioligands, the kidney received the highest absorbed dose, as expected from the biodistribution study. The absorbed dose of ^{177}Lu-L1 for the kidneys and salivary glands are low, and demonstrated fourfold higher tumor-to-kidney absorbed dose coefficients (therapeutic ratio) compared to ^{177}Lu-L9 and ^{177}Lu-L14.

Discussion

Here we investigated SAR of a new series of PSMA-targeted low-molecular-weight ^{177}Lu-labeled theranostic agents. Structural features we investigated included the presence of a *p*-halo-benzyl moiety attached to the lysine ε-amine, chelating agent, linker length and rigidity, and the attachment of an albumin-binding moiety (Fig. 1b). We also optimized aspects of the radiosynthesis and assessed short- and long-term toxicity of a lead agent, namely, ^{177}Lu-L1.

Agents synthesized here are derived from our own linker-based targeting platform [39, 40]. The attachment of a *p*-halo-benzyl moiety to the PSMA-targeting Lys-urea-Glu provided high tumor retention and fast normal tissue clearance. First, we observed significantly lower PSMA(+) cell binding affinity both in vitro and in vivo for ^{177}Lu-L7, which is without the *p*-halo-benzyl moiety, compared to ^{177}Lu-L1 and ^{177}Lu-L8, which have it. Second, we showed that radioligands with macrocyclic chelating agents DOTA-Bn-SCN (^{177}Lu-L8) and DOTAGA (^{177}Lu-L9) with four acetate donor arms provided higher tumor uptake and retention compared to the DOTAMA chelating agents (e.g., ^{177}Lu-L3 or ^{177}Lu-L1) with three acetate arms. These results were further supported by the in vitro data showing an increase in the binding affinity of L8 and L9 compared to L1. Those agents also displayed higher blood plasma protein binding compared to ^{177}Lu-L1 (Supplementary Figure 16) and also in PSMA-expressing normal tissues, including the kidneys, and salivary and lacrimal glands. Third, radioligands with the *p*-bromo-benzyl moiety showed higher tumor uptake and retention with linear linkers than when they possessed rigid linker (e.g., ^{177}Lu-L1 vs. ^{177}Lu-L11 and ^{177}Lu-L9 vs.^{177}Lu-L10). Also, no

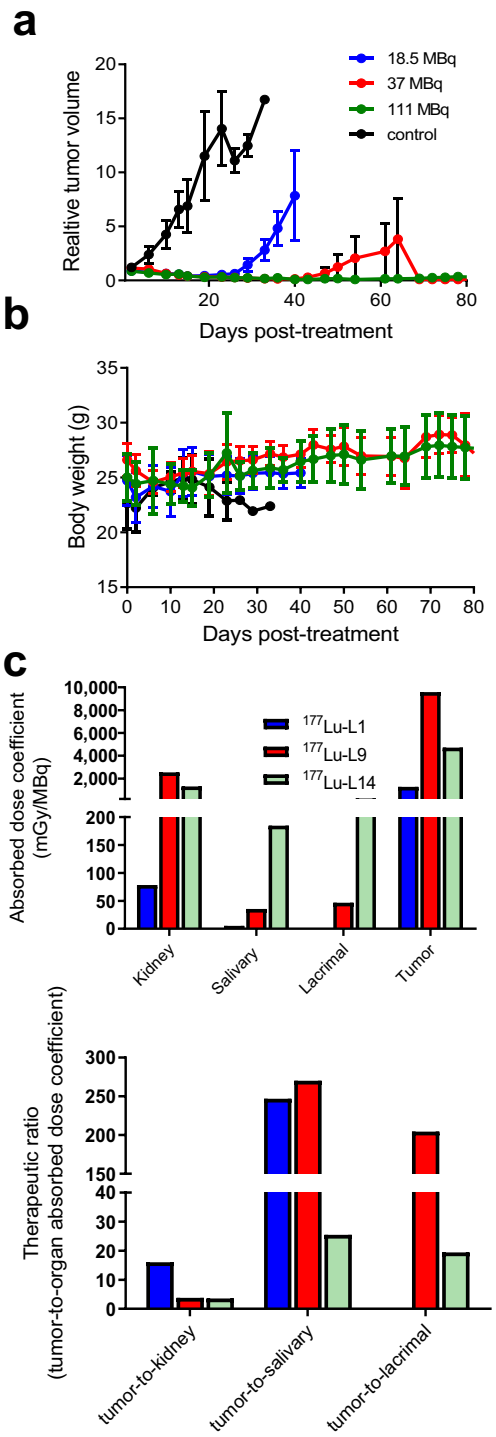

Fig. 6 Radiotherapy performed with ^{177}Lu-L1 ($n = 5$) in PSMA(+) PC3 PIP flank tumor. **a** Tumor growth curves relative to the tumor volume at day 0 (set to 1) for mice that received saline, mice treated with a single dose of 18.5 MBq, 37 MBq and 111 MBq. **b** Body weight of the corresponding treatment groups. **c** Murine radiation absorbed dose coefficients of selected organs for ^{177}Lu-L1, ^{177}Lu-L9 and ^{177}Lu-L14 (top) and therapeutic ratio (tumor-to-normal organ absorbed dose coefficients) (bottom)

significant changes were observed in tumor uptake and retention between the short vs. the long linker (^{177}Lu-L1 vs. ^{177}Lu-L5). Fourth, attachment of an albumin-binding moiety provided longer tumor retention for ^{177}Lu-L14, most likely by increasing serum half-life as recently reported by others [23–25]. That change was also associated with significantly higher kidney and salivary gland retention compared to the clinical agents ^{177}Lu-PSMA-617 (type II) or ^{177}Lu-PSMA-I&T (type I) and consistent with recent clinical data from a similar class of albumin-binding agent, ^{177}Lu-EB-PSMA-617 [41].

Several strategies have been attempted to mitigate off-target toxicity of these low-molecular-weight radioligands, such as renal protection, external cooling of salivary glands and the use of concurrently administered blocking agents [17, 42]. These radioligands are cleared through the kidneys and may be reabsorbed and partially retained in the proximal tubules, causing dose-limiting nephrotoxicity. While renal toxicity has not yet proved a major issue for ^{177}Lu-PSMA-targeted therapy, perhaps due to low reabsorption and retention of the radioligands and long-range, lowlinear energy transfer (LET) radiation of ^{177}Lu (β_{max} 0.5 MeV, 1.7 mm), a blocking strategy can be utilized to mitigate salivary or lacrimal gland irradiation for PSMA-based α-particle therapy, as seen with ^{225}Ac-PSMA-617 [43]. PSMA-based α-particle therapy can also be fraught with long-term renal toxicity [28]. The self-blocking study that we investigated showed that ^{177}Lu-L1, which already demonstrates relatively low renal uptake as a type II agent, caused no significant change in tumor uptake but yielded a tenfold kidney blockade. Another strategy to decrease off-target effects would be merely to optimize dosing regimen, i.e., amount and frequency, which is being undertaken in certain centers.

In cellulo, the colony-forming assay indicated that efficacy was directly related to cell uptake and internalization. In vivo treatment studies were conducted with larger initial tumor volumes (Supplementary Table 21) compared to similar studies in the recent literature, which used tumor sizes of 10–20 mm^3 [23]. Using large tumors could have skewed the results unfavorably due to the presence of central necrosis and more challenging dispersion of the radiotherapeutic through the tumor. Furthermore, the early deaths that we observed in the in vivo studies were not related to the animals being overcome by the tumor, but other causes not overt on autopsy [36]. Our necropsy data, while not demonstrating renal toxicity, showed acute and subacute damage to murine lacrimal glands and testes (seminiferous tubules), indicating that the lacrimal glands could be used as a surrogate organ for these ^{177}Lu-PSMA agents for preclinical toxicity evaluation. Although most preclinical studies did not report lacrimal gland uptake, an albumin-binding agent, CTT1403, displayed high uptake in the lacrimal glands [23], as anticipated.

Conclusion

We undertook an abbreviated SAR study to optimize urea-based agents for PSMA-targeted, β-particle radiopharmaceutical therapy. While difficult to alter only one variable at a time and perform studies from synthesis through long-term toxicity on all permutations, we believe that we have obtained a few hints to help guide future work. As we expect such agents to be used with increasing frequency and perhaps to maintain patients over many years, careful attention to off-target effects is necessary, although they may not have manifested in the early trials performed to date, e.g., renal toxicity. Our goal was to provide a high-affinity type II agent that was at least equivalent to existing clinical agents with respect to efficacy. Employing a *p*-bromo-benzyl moiety combined with a relatively short linker between the chelator and targeting moiety produced ^{177}Lu-L1, which likely has the most beneficial combination of structural features of this series, and could justifiably be developed for clinical use. The scaffold on which ^{177}Lu-L1 is based may also provide guidance for the corresponding α-particle emitters, which, although potentially more efficacious, may also be fraught with more imposing adverse side effects.

Acknowledgments We would like to thank Dr. R. Mease for his helpful comments.

Funding We are grateful for the following sources of support: K25 CA148901 and the Patrick C. Walsh Prostate Cancer Research Fund (SRB), CA134675, CA184228, EB024495, and the Commonwealth Foundation (MGP).

Compliance with ethical standards

Conflict of interest Drs. Banerjee and Pomper are co-inventors on one or more U.S. patents covering compounds discussed in this submission, and as such are entitled to a portion of any licensing fees and royalties generated by this technology. This arrangement has been reviewed and approved by the Johns Hopkins University in accordance with its conflict-of-interest policies. No other authors have declared any relevant conflicts of interest.

Ethical approval All animal studies were carried out in compliance with the regulations of the Johns Hopkins Animal Care and Use Committee.

Abbreviations PC, Prostate cancer; SAR, Structure–activity relationships; PSMA, Prostate-specific membrane antigen; DCIBzL, 2-[3-[1-Carboxy-5-(4-(125)I-iodo-benzoylamino)-pentyl]-ureido]-pentanedioic acid; PET, Positron emission tomography; SPECT, Single-photon emission computed tomography.

References

1. Kiess AP, Banerjee SR, Mease RC, Rowe SP, Rao A, Foss CA, et al. Prostate-specific membrane antigen as a target for cancer

imaging and therapy. Quarterly J Nucl Med Mol Imaging. 2015;59: 241–68.
2. Haberkorn U, Eder M, Kopka K, Babich JW, Eisenhut M. New strategies in prostate cancer: prostate-specific membrane antigen (PSMA) ligands for diagnosis and therapy. Clin Cancer Res. 2016;22:9–15.
3. Osborne JR, Akhtar NH, Vallabhajosula S, Anand A, Deh K, Tagawa ST. Prostate-specific membrane antigen-based imaging. Urol Oncol. 2013;31:144–54.
4. Salas Fragomeni RA, Amir T, Sheikhbahaei S, Harvey SC, Javadi MS, Solnes LB, et al. Imaging of nonprostate cancers using PSMA-targeted radiotracers: rationale, current state of the field, and a call to arms. J Nucl Med. 2018;59:871–7.
5. Chang SS, O'Keefe DS, Bacich DJ, Reuter VE, Heston WD, Gaudin PB. Prostate-specific membrane antigen is produced in tumor-associated neovasculature. Clin Cancer Res. 1999;5:2674–81.
6. Baccala A, Sercia L, Li J, Heston W, Zhou M. Expression of prostate-specific membrane antigen in tumor-associated neovasculature of renal neoplasms. Urology. 2007;70:385–90.
7. Spatz S, Tolkach Y, Jung K, Stephan C, Busch J, Ralla B, et al. Comprehensive evaluation of prostate specific membrane antigen expression in the vasculature of renal tumors: implications for imaging studies and prognostic role. J Urol. 2018;199:370–7.
8. Silver DA, Pellicer I, Fair WR, Heston WD, Cordon-Cardo C. Prostate-specific membrane antigen expression in normal and malignant human tissues. Clin Cancer Res. 1997;3:81–5.
9. Hrkach J, Von Hoff D, Ali MM, Andrianova E, Auer J, Campbell T, et al. Preclinical development and clinical translation of a PSMA-targeted docetaxel nanoparticle with a differentiated pharmacological profile. Sci Transl Med. 2012;4:128ra39.
10. Sterzing F, Kratochwil C, Fiedler H, Katayama S, Habl G, Kopka K, et al. ^{68}Ga-PSMA-11 PET/CT: a new technique with high potential for the radiotherapeutic management of prostate cancer patients. Eur J Nucl Med Mol Imaging. 2016;43:34–41.
11. Rowe SP, Macura KJ, Ciarallo A, Mena E, Blackford A, Nadal R, et al. Comparison of prostate-specific membrane antigen–based ^{18}F-DCFBC PET/CT to conventional imaging modalities for detection of hormone-naïve and castration-resistant metastatic prostate cancer. J Nucl Med. 2016;57:46–53.
12. Rahbar K, Afshar-Oromieh A, Seifert R, Wagner S, Schäfers M, Bögemann M, et al. Diagnostic performance of ^{18}F-PSMA-1007 PET/CT in patients with biochemical recurrent prostate cancer. Eur J Nucl Med Mol Imaging. 2018;45:2055–61.
13. Benesova M, Schafer M, Bauder-Wust U, Afshar-Oromieh A, Kratochwil C, Mier W, et al. Preclinical evaluation of a tailor-made DOTA-conjugated PSMA inhibitor with optimized linker moiety for imaging and endoradiotherapy of prostate cancer. J Nucl Med. 2015;56:914–20.
14. Weineisen M, Schottelius M, Simecek J, Baum RP, Yildiz A, Beykan S, et al. ^{68}Ga- and ^{177}Lu-labeled PSMA I&T: optimization of a PSMA-targeted theranostic concept and first proof-of-concept human studies. J Nucl Med. 2015;56:1169–76.
15. Fendler WP, Rahbar K, Herrmann K, Kratochwil C, Eiber M. ^{177}Lu-PSMA radioligand therapy for prostate cancer. J Nucl Med. 2017;58:1196–200.
16. Zechmann CM, Afshar-Oromieh A, Armor T, Stubbs JB, Mier W, Hadaschik B, et al. Radiation dosimetry and first therapy results with a ^{124}I/^{131}I-labeled small molecule (MIP-1095) targeting PSMA for prostate cancer therapy. Eur J Nucl Med Mol Imaging. 2014;41:1280–92.
17. Langbein T, Chausse G, Baum RP. Salivary gland toxicity of PSMA radioligand therapy: relevance and preventive strategies. J Nucl Med. 2018;59:1172–3.
18. Kopka K, Benešová M, Bařinka C, Haberkorn U, Babich J. Glu–ureido-based inhibitors of prostate-specific membrane antigen: lessons learned during the development of a novel class of low-molecular-weight theranostic radiotracers. J Nucl Med. 2017;58: 17S–26S.
19. Trover JK, Beckett ML, Wright GL. Detection and characterization of the prostate-specific membrane antigen (PSMA) in tissue extracts and body fluids. Int J Cancer. 1995;62:552–8.
20. Ray Banerjee S, Pullambhatla M, Foss CA, Falk A, Byun Y, Nimmagadda S, et al. Effect of chelators on the pharmacokinetics of (99m)Tc-labeled imaging agents for the prostate-specific membrane antigen (PSMA). J Med Chem. 2013;56:6108–21.
21. Banerjee SR, Pullambhatla M, Foss CA, Nimmagadda S, Ferdani R, Anderson CJ, et al. ^{64}Cu-labeled inhibitors of prostate-specific membrane antigen for PET imaging of prostate cancer. J Med Chem. 2014;57:2657–69.
22. Eder M, Schaefer M, Bauder-Wuest U, Hull W-E, Waengler C, Mier W, et al. ^{68}Ga-complex lipophilicity and the targeting property of a urea-based PSMA inhibitor for PET imaging. Bioconjug Chem. 2012;23:688–97.
23. Choy CJ, Ling X, Geruntho JJ, Beyer SK, Latoche JD, Langton-Webster B, et al. ^{177}Lu-labeled phosphoramidate-based PSMA inhibitors: the effect of an albumin binder on biodistribution and therapeutic efficacy in prostate tumor-bearing mice. Theranostics. 2017;7:1928–39.
24. Umbricht CA, Benesova M, Schibli R, Muller C. Preclinical development of novel PSMA-targeting radioligands: modulation of albumin-binding properties to improve prostate cancer therapy. Mol Pharm. 2018;15:2297–306.
25. Kelly J, Amor-Coarasa A, Ponnala S, Nikolopoulou A, Williams C Jr, Schlyer D, et al. Trifunctional PSMA-targeting constructs for prostate cancer with unprecedented localization to LNCaP tumors. Eur J Nucl Med Mol Imaging. 2018.2018;45:1841–1851.
26. Banerjee SR, Foss CA, Pullambhatla M, Wang Y, Srinivasan S, Hobbs RF, et al. Preclinical evaluation of ^{86}Y-labeled inhibitors of prostate-specific membrane antigen for dosimetry estimates. J Nucl Med. 2015;56:628–34.
27. Chen Y, Foss CA, Byun Y, Nimmagadda S, Pullambahatla M, Fox JJ, et al. Radiohalogenated prostate-specific membrane antigen (PSMA)-based ureas as imaging agents for prostate cancer. J Med Chem. 2008;51:7933–43.
28. Kiess AP, Minn I, Vaidyanathan G, Hobbs RF, Josefsson A, Shen C, et al. (2S)-2-(3-(1-Carboxy-5-(4-211At-astatobenzamido)pentyl)ureido)-pentanedioic acid for PSMA-targeted alpha-particle radiopharmaceutical therapy. J Nucl Med. 2016;57:1569–75.
29. Banerjee SR, Pullambhatla M, Byun Y, Nimmagadda S, Foss CA, Green G, et al. Sequential SPECT and optical imaging of experimental models of prostate cancer with a dual modality inhibitor of the prostate-specific membrane antigen. Angew Chem Int Ed. 2011;50:9167–70.
30. Ray Banerjee S, Chen Z, Pullambhatla M, Lisok A, Chen J, Mease RC, et al. Preclinical comparative study of ^{68}Ga-labeled DOTA, NOTA, and HBED-CC chelated radiotracers for targeting PSMA. Bioconjug Chem. 2016;27:1447–55.
31. Kiess AP, Minn I, Chen Y, Hobbs R, Sgouros G, Mease RC, et al. Auger radiopharmaceutical therapy targeting prostate-specific membrane antigen. J Nucl Med. 2015;56:1401–7.
32. Chen Y, Chatterjee S, Lisok A, Minn I, Pullambhatla M, Wharram B, et al. A PSMA-targeted theranostic agent for photodynamic therapy. J Photochem Photobiol B Biol. 2017;167:111–6.
33. Fendler WP, Stuparu AD, Evans-Axelsson S, Luckerath K, Wei L, Kim W, et al. Establishing ^{177}Lu-PSMA-617 radioligand therapy in a syngeneic model of murine prostate cancer. J Nucl Med. 2017;58: 1786–92.
34. Bouchet LG, Bolch WE, Blanco HP, Wessels BW, Siegel JA, Rajon DA, et al. MIRD Pamphlet No. 19: absorbed fractions and

radionuclide S values for six age-dependent multiregion models of the kidney. J Nucl Med. 2003;44:1113–47.
35. Olszewski RT, Bukhari N, Zhou J, Kozikowski AP, Wroblewski JT, Shamimi-Noori S, et al. NAAG peptidase inhibition reduces locomotor activity and some stereotypes in the PCP model of schizophrenia via group II mGluR. J Neurochem. 2004;89:876–85.
36. Brayton C. Chapter 25 - spontaneous diseases in commonly used mouse strains. In: Fox JG, Davisson MT, Quimby FW, Barthold SW, Newcomer CE, Smith AL, editors. The mouse in biomedical research. second ed. Burlington: Academic; 2007. p. 623–717.
37. Brayton CF, Treuting PM, Ward JM. Pathobiology of aging mice and GEM: background strains and experimental design. Vet Pathol. 2012;49:85–105.
38. Serfilippi LM, Pallman DR, Russell B. Serum clinical chemistry and hematology reference values in outbred stocks of albino mice from three commonly used vendors and two inbred strains of albino mice. Contemp Top Lab Anim Sci. 2003;42:46–52.
39. Banerjee SR, Foss CA, Castanares M, Mease RC, Byun Y, Fox JJ, et al. Synthesis and evaluation of technetium-99m- and rhenium-labeled inhibitors of the prostate-specific membrane antigen (PSMA). J Med Chem. 2008;51:4504–17.
40. Ray Banerjee S, Pullambhatla M, Foss CA, Falk A, Byun Y, Nimmagadda S, et al. Effect of chelators on the pharmacokinetics of ^{99m}Tc-labeled imaging agents for the prostate-specific membrane antigen (PSMA). J Med Chem. 2013;56:6108–21.
41. Zang J, Fan X, Wang H, Liu Q, Wang J, Li H, et al. First-in-human study of ^{177}Lu-EB-PSMA-617 in patients with metastatic castration-resistant prostate cancer. Eur J Nucl Med Mol Imaging. 2019;46:148–58.
42. Taïeb D, Foletti J-M, Bardiès M, Rocchi P, Hicks RJ, Haberkorn U. PSMA-targeted radionuclide therapy and salivary gland toxicity: why does it matter? J Nucl Med. 2018;59:747–8.
43. Kratochwil C, Bruchertseifer F, Rathke H, Bronzel M, Apostolidis C, Weichert W, et al. Targeted alpha therapy of mCRPC with ^{225}Actinium-PSMA-617: dosimetry estimate and empirical dose finding. J Nucl Med. 2017;58:1624–31.